

# A general strategy for nanocrystal synthesis

Xun Wang<sup>1,2</sup>, Jing Zhuang<sup>1,2</sup>, Qing Peng<sup>1,2</sup> & Yadong Li<sup>1,2</sup>

**New strategies for materials fabrication are of fundamental importance in the advancement of science and technology<sup>1–12</sup>. Organometallic<sup>13,14</sup> and other organic solution phase<sup>15–17</sup> synthetic routes have enabled the synthesis of functional inorganic quantum dots or nanocrystals. These nanomaterials form the building blocks for new bottom-up approaches to materials assembly for a range of uses; such materials also receive attention because of their intrinsic size-dependent properties and resulting applications<sup>18–21</sup>. Here we report a unified approach to the synthesis of a large variety of nanocrystals with different chemistries and properties and with low dispersity; these include noble metal, magnetic/dielectric, semiconducting, rare-earth fluorescent, biomedical, organic optoelectronic semiconducting and conducting polymer nanoparticles. This strategy is based on a general phase transfer and separation mechanism occurring at the interfaces of the liquid, solid and solution phases present during the synthesis. We believe our methodology provides a simple and convenient route to a variety of building blocks for assembling materials with novel structure and function in nanotechnology<sup>13–29</sup>.**

We chose noble metals as an example to demonstrate the effectiveness of this method in yielding high quality nanocrystals. Uniform noble metal quantum dots, or nanocrystals, can be obtained through the reduction of noble metal ions by ethanol at a temperature of 20 to 200 °C under hydrothermal or atmospheric conditions. In a typical synthesis, 20 ml of aqueous solution containing noble metal salts (for example, 0.5 g of AgNO<sub>3</sub>, HAuCl<sub>4</sub> or other soluble chlorides), 1.6 g sodium linoleate, 10 ml ethanol and 2 ml linoleic acid were added to a 40 ml autoclave tube under agitation. The reactions were controlled at different temperatures for specific metals, for example, 80 to 200 °C for Ag, 20 to 200 °C for Ru, Rh and Ir, 20 to 100 °C for Au, Pd and Pt. The system was sealed and treated at the designated temperature for 10 hours. After the reaction was cooled to room temperature, the products were collected at the bottom of the vessel. Based on the same synthetic process, other fatty acid and corresponding salt systems can play the same roles as the linoleic acid system.

Figure 1a shows transmission electron microscope (TEM) images of typical samples of Ag, Au, Rh and Ir nanocrystals and indicates the large quantity and good uniformity (see Supplementary Information Part I and II) that were achieved using this approach. The Ag and Au nanocrystals are usually in round shapes with smooth surfaces, and self-assemble into ordered two-dimensional (2D) arrays on the surface of the TEM grid (Fig. 1a). The diameters of the nanocrystals can be reasonably tuned from about 4 to 15 nm by altering temperature, the mole ratio of the protecting reagents to noble metal ions or the chain length of the fatty acid (see Supplementary Information Part III). This approach has also been shown to yield the nearly monodisperse ultrafine metal nanocrystals of Ru, Rh, Ir, Pd and Pt with diameters of approximately 3 nm or less. Thorough high resolution (HR) TEM characterizations revealed the highly crystalline nature of these nanocrystals. Typical HRTEM images of Ir nanocrystals with diameters ~1.7 nm show an interplanar spacing

of ~0.22 nm, which corresponds to the (111) planes of face-centred cubic Ir. EDS (energy dispersive spectroscopy) microanalysis and powder XRD (X-ray diffraction) (Fig. 2a) measurement have proven the successful synthesis of face-centred cubic structured Ag (JCPDS 4-783), Au (JCPDS 4-784), Pd (JCPDS 46-1043), Pt (JCPDS 4-802), Rh (JCPDS 5-685), Ir (JCPDS 46-1044) and hexagonal Ru (JCPDS 6-663).

The primary reaction in the preparation of noble metal nanocrystals through this liquid–solid–solution (LSS) process involved the reduction of noble metal ions by ethanol at the interfaces of metal linoleate (solid), ethanol–linoleic acid liquid phase (liquid) and water–ethanol solutions (solution) at different designated temperatures (Fig. 3). After the aqueous solution of noble metal ions, sodium linoleate (or another sodium stearate) and the mixture of linoleic acid (or another fatty acid) and ethanol were added into the vessel in order. Three phases formed in this system: sodium linoleate (solid), the liquid phase of ethanol and linoleic acid (liquid), and the water–ethanol solution containing noble metal ions (solution). A phase transfer process of the noble metal ions occurred spontaneously across the interface of sodium linoleate (solid) and the water–ethanol solution (solution) based on ion exchange, which led to the formation of noble metal linoleate and the entering of the sodium ions into the aqueous phases. Then at a designated temperature, the ethanol in the liquid and solution phases reduced the noble metal ions at the liquid–solid or solution–solid interfaces. Along with the reduction process, the *in-situ* generated linoleic acid absorbed on the surface of the noble metal nanocrystals with the alkyl chains on the outside, through which the produced metal nanocrystals will gain hydrophobic surfaces. A spontaneous phase-separation process then occurred because of the weight of the metal nanocrystals and the incompatibility between the hydrophobic surfaces and their hydrophilic surroundings, and the noble metal nanocrystals can be easily collected at the bottom of the container.

This LSS phase transfer and separation process can generate nanocrystals with a variety of properties such as, semiconducting, fluorescent, magnetic and dielectric. The phase transfer process can occur for nearly all the transitional or main group metal ions, which gives flexibility to the reactions at the interfaces (see Supplementary Information Part IV). After the phase transfer process of the metal ions from aqueous solution to the solid phase of (RCOO)<sub>n</sub>M, under designated reaction conditions, the M<sup>n+</sup> dehydrates into oxides (to yield for example, TiO<sub>2</sub>, CuO, ZrO<sub>2</sub>, SnO<sub>2</sub> or ZnO) and/or composite oxides (to yield for example, MFe<sub>2</sub>O<sub>4</sub> (M represents Fe, Co, Mg, Zn or Mn) and MTiO<sub>3</sub> (M represents Ba or Sr) through co-precipitation). Alternatively, M<sup>n+</sup> might react with other anion species such as S<sup>2-</sup> (S<sup>2-</sup> was supplied by Na<sub>2</sub>S or (NH<sub>4</sub>)<sub>2</sub>S, to yield for example CdS, MnS, PbS, Ag<sub>2</sub>S, CuS or ZnS), Se<sup>2-</sup> (Se<sup>2-</sup> was generated by the reduction of SeO<sub>3</sub><sup>2-</sup> by N<sub>2</sub>H<sub>4</sub>, to yield for example CdSe or ZnSe) or F<sup>-</sup> (F<sup>-</sup> was provided from NaF or NH<sub>4</sub>F, to yield for example YF<sub>3</sub>, LaF<sub>3</sub> or NaYF<sub>4</sub>) to yield various functional nanocrystals.

Nearly all the bandgap semiconductors can be effectively prepared through this simple LSS phase transfer and separation method, such

<sup>1</sup>Department of Chemistry, Tsinghua University, <sup>2</sup>National Center for Nanoscience and Nanotechnology, Beijing, 100084 China.

as  $\text{TiO}_2$ ,  $\text{CuO}$ ,  $\text{ZrO}_2$ ,  $\text{SnO}_2$ ,  $\text{CdS}$ ,  $\text{Ag}_2\text{S}$ ,  $\text{ZnS}$ ,  $\text{PbS}$ ,  $\text{MnS}$ ,  $\text{ZnSe}$  and  $\text{CdSe}$ . Representative TEM images of typical semiconductors of  $\text{Ag}_2\text{S}$ ,  $\text{PbS}$ ,  $\text{ZnSe}$ ,  $\text{CdSe}$  and  $\text{TiO}_2$  show the successful synthesis of various uniform semiconductor nanocrystals through this LSS approach (Fig. 1b, c). Two-dimensional assembly of  $\text{PbS}$ ,  $\text{Ag}_2\text{S}$ ,  $\text{CuO}$ ,  $\text{ZnSe}$  and  $\text{CdSe}$  nanocrystals occurred spontaneously on the copper TEM grids after the evaporation of the solvents, indicating the regular shapes and narrow size distributions of these nanocrystals. Similar to the synthesis of noble metal nanocrystals, the size of the semiconductor nanocrystals can be tuned through several factors including temperature, mole ratio and the length of alkyl chains (see Supplementary Information Part III), however, for the synthesis of selenides, the temperature was controlled above  $120^\circ\text{C}$  to ensure the complete reduction of  $\text{SeO}_3^{2-}$  by  $\text{N}_2\text{H}_4$  (Fig. 2b). As mentioned above, the phase transfer process and control of the reactions at the different interfaces enabled the monodispersity and variability of the semiconductor nanocrystals obtained.

By adopting bi-metal precursors in a certain mole ratio, composite oxide nanocrystals such as magnetic  $\text{MFe}_2\text{O}_4$  ( $M$  represents  $\text{Fe}$ ,  $\text{Co}$ ,  $\text{Mg}$ ,  $\text{Zn}$  or  $\text{Mn}$ ) and dielectric  $\text{MTiO}_3$  ( $M$  represents  $\text{Ba}$  or  $\text{Sr}$ ) can be effectively prepared through co-precipitation reactions following this

LSS phase transfer and separation method. Uniform nanocrystals of magnetic spinel  $\text{MFe}_2\text{O}_4$  could be prepared through the coprecipitation of  $\text{Fe}^{2+}$  ions and  $\text{Fe}^{3+}$ ,  $\text{Co}^{2+}$ ,  $\text{Mg}^{2+}$ ,  $\text{Mn}^{2+}$  and  $\text{Zn}^{2+}$  ions. As shown in Fig. 1c, magnetic nanocrystals of  $\text{Fe}_3\text{O}_4$  and  $\text{CoFe}_2\text{O}_4$  with diameters  $\sim 10$  nm formed 2D patterns on the TEM grids and showed good uniformity, which will be useful in biological labelling fields. In a similar way, the reaction between  $\text{Ti}^{4+}$  and  $\text{Ba}^{2+}$  and/or  $\text{Sr}^{2+}$  under strong alkali conditions can be used to prepare uniform nanocrystals of  $\text{BaTiO}_3$  and  $\text{SrTiO}_3$ . Typical TEM and XRD analyses are shown in Fig. 1c and Fig. 2c, respectively, and show the formation of uniform nanocrystals of tetragonal  $\text{BaTiO}_3$  (JCPDS 74-1960) with diameters  $\sim 17$  nm.

Our LSS phase transfer and separation approach can also be used in generating nearly monodisperse rare earth fluorescent nanocrystals with up-conversion or down-conversion emission properties. These nanocrystals can also be prepared by tuning the reaction at the interfaces of the different phases. For example, after the phase transfer process of the rare earth ions, the reaction between  $\text{NaF}$  and the  $(\text{RCOO})_n\text{Ln}$  generates  $\text{LnF}_3$  ( $\text{NaYF}_4$  in the case of  $\text{Y}$ ; the reaction between  $\text{NH}_4\text{F}$  and  $\text{Y}^{3+}$  yields  $\text{YF}_3$ ), whereas the reaction between  $\text{OH}^-$  and  $(\text{RCOO})_n\text{Ln}$  generates  $\text{Ln}(\text{OH})_3$  nanocrystals (Fig. 2d).

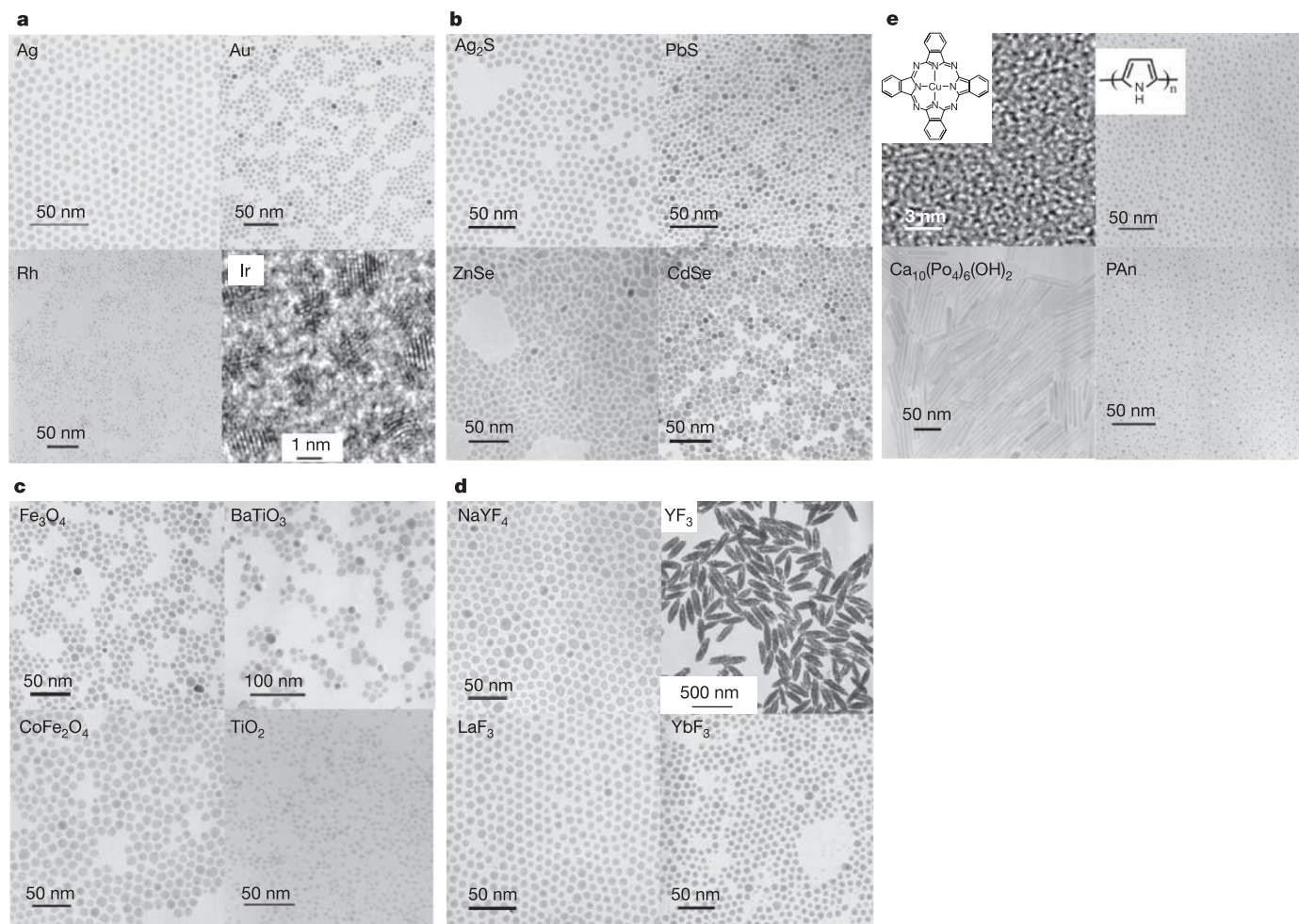


**Figure 1 | TEM images of nanocrystals.** **a**, Noble metal nanocrystals:  $\text{Ag}$  ( $6.1 \pm 0.3$  nm;  $90^\circ\text{C}$ ),  $\text{Au}$  ( $7.1 \pm 0.5$  nm;  $50^\circ\text{C}$ ),  $\text{Rh}$  ( $2.2 \pm 0.1$  nm;  $120^\circ\text{C}$ ) and  $\text{Ir}$  ( $1.7 \pm 0.09$  nm;  $120^\circ\text{C}$ ). **b**, Semiconductor nanocrystals:  $\text{Ag}_2\text{S}$  ( $7.3 \pm 0.4$  nm;  $120^\circ\text{C}$ ;  $\text{Ag}^+:\text{S}^{2-}$ , 2:1),  $\text{PbS}$  ( $5.7 \pm 0.2$  nm;  $\text{Pb}^{2+}:\text{S}^{2-}$ , 1:1),  $\text{ZnSe}$  ( $8.2 \pm 0.9$  nm;  $\text{Zn}^{2+}:\text{SeO}_3^{2-}$ , 1:1;  $180^\circ\text{C}$ ) and  $\text{CdSe}$  ( $7.1 \pm 0.8$  nm;  $\text{Cd}^{2+}:\text{SeO}_3^{2-}$ , 1:1;  $180^\circ\text{C}$ ). **c**, Magnetic and dielectric nanocrystals:  $\text{Fe}_3\text{O}_4$  ( $9.1 \pm 0.8$  nm;  $\text{Fe}^{2+}:\text{Fe}^{3+}$ , 1:2;  $160^\circ\text{C}$ ),  $\text{CoFe}_2\text{O}_4$  ( $11.5 \pm 0.6$  nm;  $\text{Co}^{2+}:\text{Fe}^{2+}$ , 1:2;  $180^\circ\text{C}$ ),  $\text{BaTiO}_3$  ( $16.8 \pm 1.7$  nm; 7 g  $\text{NaOH}$  for 0.5 g  $\text{Ba}(\text{NO}_3)_2$  and equal amount of  $\text{TiCl}_3$  (in mole ratio);  $180^\circ\text{C}$ ;  $\text{Ti}^{3+}$  have been adopted as  $\text{Ti}$

sources because of the relative stability of  $\text{Ti}^{3+}$  to  $\text{Ti}^{4+}$  under aqueous conditions, which will be oxidized into  $\text{Ti}^{4+}$  under hydrothermal conditions) and  $\text{TiO}_2$  ( $4.3 \pm 0.2$  nm; 1 ml 30%  $\text{TiCl}_3$  solution for 40 ml vessel;  $180^\circ\text{C}$ ). **d**, Rare earth fluorescence nanocrystals:  $\text{NaYF}_4$  ( $10.5 \pm 0.7$  nm;  $\text{NaF}:\text{Y}^{3+}$ , 4:1,  $180^\circ\text{C}$ ),  $\text{YF}_3$  ( $\text{NH}_4\text{F}:\text{Y}^{3+}$ , 3:1,  $180^\circ\text{C}$ ),  $\text{LaF}_3$  ( $8.0 \pm 0.3$  nm;  $\text{F}^-:\text{La}^{3+}$ , 3:1,  $180^\circ\text{C}$ ),  $\text{YbF}_3$  ( $9.5 \pm 0.6$  nm;  $\text{F}^-:\text{Yb}^{3+}$ , 3:1,  $180^\circ\text{C}$ ). **e**, TEM images of  $\text{Ca}_{10}(\text{PO}_4)_6(\text{OH})_2$ , Ppy ( $4.2 \pm 0.5$  nm), PAn ( $3.3 \pm 0.5$  nm) and copper phthalocyanine ( $0.8 \pm 0.1$  nm) nanocrystals.

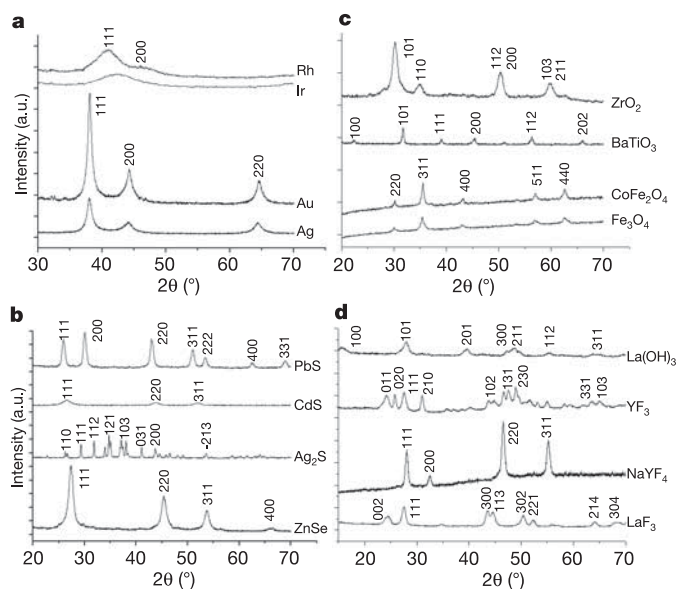


**Figure 2 | XRD patterns of nanocrystals.** **a**, Noble metal nanocrystals: Au, Ag, Rh and Ir. **b**, Semiconductor nanocrystals: monoclinic  $\text{Ag}_2\text{S}$  (JCPDS 14-0072), face-centred cubic PbS (JCPDS 5-592), ZnSe (JCPDS 80-21) and face-centred cubic CdS (JCPDS 75-0581). **c**, Magnetic and dielectric nanocrystals:  $\text{Fe}_3\text{O}_4$  (JCPDS 76-1849),  $\text{CoFe}_2\text{O}_4$  (JCPDS 79-1744), tetragonal  $\text{BaTiO}_3$  (JCPDS 74-1960) and  $\text{ZrO}_2$ . **d**, Rare earth fluorescence nanocrystals:  $\text{NaYF}_4$  (JCPDS 77-2042),  $\text{YF}_3$  (JCPDS 74-911),  $\text{LaF}_3$  (JCPDS 72-1435) and  $\text{La(OH)}_3$  (JCPDS 36-1481).

Figure 1d shows the TEM figures of  $\text{NaYF}_4$ ,  $\text{YF}_3$ ,  $\text{LaF}_3$  and  $\text{YbF}_3$  nanocrystals.  $\text{NaYF}_4$ ,  $\text{YbF}_3$  and  $\text{LaF}_3$  are approximately round, with a diameter in the range of 4–12 nm (that varies with temperature), whereas  $\text{YF}_3$  is characterized as having a rice-like shape with a diameter  $\sim 100$  nm and length  $\sim 500$  nm (composed of uniform nanocrystals with a diameter  $\sim 5$  nm).  $\text{Ln(OH)}_3$  products are usually composed of uniform nanorods with a diameter 3–15 nm (that varies with temperature). By doping different rare earth ions such as  $\text{Eu}^{3+}$ ,  $\text{Tb}^{3+}$  or Yb/Er these nanocrystals were functional as fluorescence nanocrystals (see Supplementary Information part V).

Along with the series of functional nanocrystals mentioned above, this LSS strategy also shows great potential in the synthesis of a broad range of new-type nanocrystals and/or nanoparticles (see Supplementary Information part VI). This will provide new materials

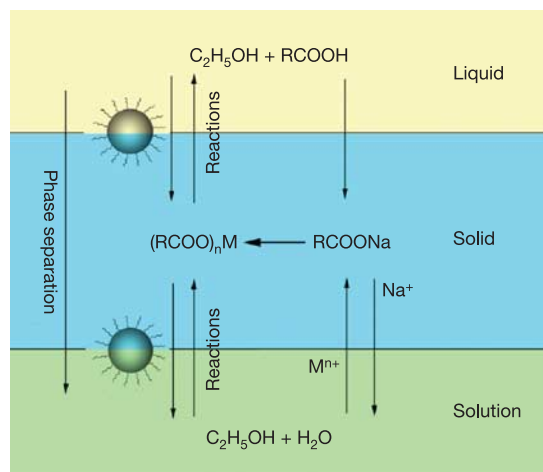


**Figure 3 | Scheme of liquid-solid-solution (LSS) phase transfer synthetic strategy.**

for wide research areas including biocompatible materials, organic optoelectronic semiconductors, nanomedicine as well as conducting polymers. For example, the monodisperse biocompatible hydroxyapatite ( $\text{Ca}_{10}(\text{PO}_4)_6(\text{OH})_2$ ) nanorods (Fig. 1e, bottom left), which as a raw material may find an application in the preparation of artificial bone grafts because of its uniformity and nanometre size. Also, the typical conducting polymer nanocrystals of PPy and PAN (Fig. 1e, right), may provide an ideal model for the investigation of nano-size effects in the conducting polymer field. Finally, metal (copper in this case) phthalocyanine nanocrystals (Fig. 1e, top left) obtained following this LSS procedure, can be further investigated as an optoelectronic nanomaterial. Therefore, by properly tuning the chemical reactions at the interfaces, we believe that more interesting and important new-type nanocrystals can be obtained.

All the nanocrystals (such as noble metal, magnetic, dielectric, semiconducting and rare earth fluorescence), and other new type (such as, monodisperse biomedical, organic optoelectronic semiconductors and conducting polymers) nanoparticles, can be easily dispersed in nonpolar solvents (such as, cyclohexane or chloroform) to form homogenous colloidal solutions (Fig. 4), which are usually stable for months. By dropping the solution on the surface of a

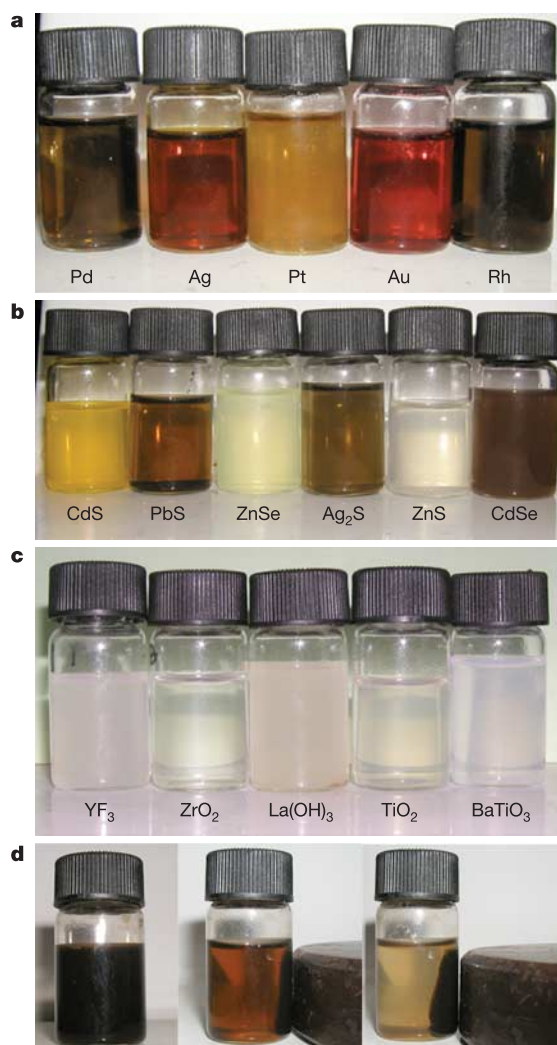


**Figure 4 | Cyclohexane solutions of nanoparticles with a typical concentration of 2%.** **a–d**, Cyclohexane solutions of noble metal (**a**), semiconductors (**b**), rare earth fluorescence (**c**) and magnetic nanocrystals (**d**). **d**, The separation of  $\text{CoFe}_2\text{O}_4$  nanocrystals from the bulky solution by magnetic force.

substrate or through a dip-coating technique, monolayer films of functional nanocrystals could be easily obtained, which will greatly increase their application in nanoscience and technology. These nanocrystals could also be re-precipitated and separated by adding an appropriate amount of ethanol to the bulky nanocrystals solutions or by force due to an external field and show advantages in processing. All these disperse/separation characteristics of the functional nanocrystals obtained through this LSS approach will provide the building blocks for the bottom-up approach to nanoscale fabrication in nanosciences and nanotechnologies.

Received 18 May; accepted 23 June 2005.

1. Kroto, H. W., Heath, J. R., O'Brien, S. C., Curl, R. F. & Smalley, R. E. C60: Buckminsterfullerene. *Nature* **318**, 162–163 (1985).
2. Iijima, S. Helical microtubules of graphitic carbon. *Nature* **354**, 56–58 (1991).
3. Morales, A. M. & Lieber, C. M. A laser ablation method for the synthesis of crystalline semiconductor nanowires. *Science* **279**, 208–211 (1998).
4. Huang, M. H. *et al.* Room-temperature ultraviolet nanowire nanolasers. *Science* **292**, 1897–1899 (2001).
5. Tenne, R., Margulis, L., Genut, M. & Hodes, G. Polyhedral and cylindrical structures of Tungsten disulfide. *Nature* **360**, 444–446 (1992).
6. Pan, Z. W., Dai, Z. R. & Wang, Z. L. Nanobelts of semiconducting oxides. *Science* **291**, 1947–1949 (2001).
7. Duan, X. F., Huang, Y., Cui, Y., Wang, J. F. & Lieber, C. M. Indium phosphide nanowire as building blocks for nanoscale electronic and optoelectronic devices. *Nature* **409**, 66–69 (2001).
8. Huang, Y., Duan, X. F., Wei, Q. Q. & Lieber, C. M. Directed assembly of one-dimensional nanostructures into functional networks. *Science* **291**, 630–633 (2001).
9. Law, M. *et al.* Nanoribbon waveguides for subwavelength photonics integration. *Science* **305**, 1269–1273 (2004).
10. Beck, J. S. *et al.* A new family of mesoporous molecular sieves prepared with liquid crystal templates. *J. Am. Chem. Soc.* **114**, 10834–10843 (1992).
11. Huo, Q. S. *et al.* Generalized syntheses of periodic surfactant inorganic composite-materials. *Nature* **368**, 317–321 (1994).
12. Yang, P. D., Zhao, D. Y., Margolese, D. I., Chmelka, B. F. & Stucky, G. D. Generalized syntheses of large-pore mesoporous metal oxides with semicrystalline frameworks. *Nature* **396**, 152–155 (1998).
13. Murray, C. B., Norris, D. J. & Bawendi, M. G. Synthesis and characterization of nearly monodisperse CdE (E = sulfur, selenium, tellurium) semiconductor nanocrystallites. *J. Am. Chem. Soc.* **115**, 8706–8715 (1993).
14. Peng, X. G. *et al.* Shape control of CdSe nanocrystals. *Nature* **404**, 59–61 (2000).
15. Sun, S. H., Murray, C. B., Weller, D., Folks, L. & Moser, A. Monodisperse FePt nanoparticles and ferromagnetic FePt nanocrystal superlattices. *Science* **287**, 1989–1992 (2000).
16. Murray, C. B., Kagan, C. R. & Bawendi, M. G. Self organization of CdSe nanocrystallites into 3-dimensional quantum-dot superlattices. *Science* **270**, 1335–1338 (1995).
17. Sun, Y. G. & Xia, Y. N. Shape-controlled synthesis of gold and silver nanoparticles. *Science* **298**, 2176–2179 (2002).
18. Jovin, T. M. Quantum dots finally come of age. *Nature Biotechnol.* **21**, 32–33 (2003).
19. Huynh, W. U., Dittmer, J. J. & Alivisatos, A. P. Hybrid nanorod-polymer solar cells. *Science* **295**, 2425–2427 (2002).
20. Tessler, N., Medvedev, V., Kazes, M., Kan, S. H. & Banin, U. Efficient near-infrared polymer nanocrystal light-emitting diodes. *Science* **295**, 1506–1508 (2002).
21. Klimov, V. I. *et al.* Optical gain and stimulated emission in nanocrystal quantum dots. *Science* **290**, 314–317 (2000).
22. Li, Y. D. *et al.* Bismuth nanotubes: A rational low-temperature synthetic route. *J. Am. Chem. Soc.* **123**, 9904–9905 (2001).
23. Li, Y. D., Li, X. L., He, R. R., Zhu, J. & Deng, Z. X. Artificial lamellar mesostructures to WS<sub>2</sub> nanotubes. *J. Am. Chem. Soc.* **124**, 1411–1416 (2002).
24. Wang, X. & Li, Y. D. Selected-control hydrothermal synthesis of alpha- and beta-MnO<sub>2</sub> single crystal nanowires. *J. Am. Chem. Soc.* **124**, 2880–2881 (2002).
25. Wang, X. & Li, Y. D. Synthesis and characterization of lanthanide hydroxide single-crystal nanowires. *Angew. Chem. Int. Edn Engl.* **41**, 4790–4793 (2002).
26. Peng, Q., Dong, Y. J. & Li, Y. D. ZnSe semiconductor hollow microspheres. *Angew. Chem. Int. Edn Engl.* **42**, 3027–3030 (2003).
27. Wang, X. & Li, Y. D. Fullerene-like rare-earth nanoparticles. *Angew. Chem. Int. Edn Engl.* **42**, 3497–3500 (2003).
28. Wang, X., Zhuang, J., Chen, J., Zhou, K. B. & Li, Y. D. Thermally stable silicate nanotubes. *Angew. Chem. Int. Edn Engl.* **43**, 2017–2020 (2004).
29. Sun, X. M. & Li, Y. D. Ga<sub>2</sub>O<sub>3</sub> and GaN semiconductor hollow spheres. *Angew. Chem. Int. Edn Engl.* **43**, 3827–3831 (2004).

**Supplementary Information** is linked to the online version of the paper at [www.nature.com/nature](http://www.nature.com/nature).

**Acknowledgements** This work was supported by NSFC, the Foundation for the Author of National Excellent Doctoral Dissertation of China and the State Key Project of Fundamental Research for Nanomaterials and Nanostructures.

**Author Information** Reprints and permissions information is available at [npg.nature.com/reprintsandpermissions](http://npg.nature.com/reprintsandpermissions). The authors declare no competing financial interests. Correspondence and requests for materials should be addressed to L.Y. ([ydli@tsinghua.edu.cn](mailto:ydli@tsinghua.edu.cn)).